Theoretical and Experimental Investigation of the Modulated Scattering Antenna Array for Mobile Terminal Applications

Mang He, *Member, IEEE*, Lin Wang, Qiang Chen, *Member, IEEE*, Qiaowei Yuan, and Kunio Sawaya, *Senior Member, IEEE*

***Abstract*—The performance of the modulated scattering antenna array (MSAA) for mobile terminals is investigated in this paper. The electromagnetic scattering of the modulated scattering elements (MSEs) loaded with Schottky diode is analyzed by using the Volterra series method in conjunction with the method of moments, which rigorously includes the mutual couplings among the MSAA elements. By virtue of closed-form analytical expression of Volterra analysis, useful physical insights and guidelines are provided to find optimum parameters of the MSEs in order to improve the performance of the MSAA for wireless communications. Parametrical studies are carried out for the purpose of enhancing the scattered power level of the second-order intermodulation caused by the nonlinear load in the MSEs. Both numerical simulations and experiments validate the proposed theoretical analysis.**

***Index Terms*—Modulated scattering antenna array (MSAA), modulated scattering element (MSE), nonlinear circuits, method of moments (MoM), Volterra series.**

I. Introduction

THE MODULATED scattering technique was firstly presented by Richmond to improve the accuracy of measurement of electric fields [1]. Recently, based on this technique, Yuan *et al.* proposed a new concept, called the modulated scattering antenna array (MSAA), and utilized it as a receiving antenna array for the mobile terminals in the multiple-input multiple-output (MIMO) communication systems [2]. In this configuration of the MSAA, only one branch of front-end circuits is needed in the normal receiving antenna, and other output signals required in the MIMO channel are realized by using the scattered fields of the second-order mixing product from the modulated scattering elements (MSEs) loaded with nonlinear devices. Therefore, the MSAA is particularly useful for mobile handsets in which compactness of the receiving antennas is of primary importance because the MSAA saves the complex front-end circuits for most receiving antenna elements, although it provides slightly inferior performance compared to the commonly used antenna array in MIMO systems [2]–[4]. The performance degradation of the MSAA is mainly due to the low power level of the modulated scattering field received by the normal receiving antenna to which the front-end circuit is connected [2]. Therefore, how to improve the modulated scattering power level from MSEs is extremely important for the applications of the MSAA to MIMO system and is the major focus of this paper.

In the authors' previous work [2]–[4], the performance of the MSAA in the wireless communication systems has been extensively studied through experiments in terms of the spatial diversity, the channel capacity, and the error vector magnitude (EVM) in Rayleigh fading environments. However, a theoretical analysis method has not been provided yet to systematically investigate and further improve the performance of a MSAA system. In this paper, a rigorous and accurate analysis of the MSAA is presented based on the Volterra-series method and the method of moments (MoM), which aims at optimizing the parameters of the MSAA and further improving its performance.

This paper is organized as follows. In Section II, the basic configuration and features of the MSAA are introduced, and the theoretical analysis of a two-element MSAA with diode loads based on the Volterra-series method and MoM are presented. InSection III, both numerical and experimental parametrical studies are carried out, and several effective means to increase the scattered power level of the second-order intermodulation from MSEs are discussed in detail.

II. MSAA Configuration and Analysis Method

A. Configuration of the MSAA

Fig. 1 shows the configuration of a typical MSAA loaded with diodes. The MSAA consists of two types of elements: one is a normal receiving antenna and the others are MSEs. Only one branch of the RF receiver is connected to the normal antenna element, while the MSEs do not have their own receiving circuits. The MSEs can be seen as antennas or scatterers that are loaded with the nonlinear devices and are fed by local signals with low-frequency $f_{\mathrm{LO}n}$.

When the incident signal with the frequency f_{RF} impinges the MSAA, the scattered fields with new mixing frequencies will be produced due to the nonlinear loads connected to the MSEs and will be received by the normal receiving antenna that

Manuscript received April 14, 2010; revised July 22, 2010; accepted July 23, 2010. Date of publication September 02, 2010; date of current version October 13, 2010. This work was supported in part by the National Science Foundation of China under Grant 60801008, and in part by the Global COE Program of Tohoku University, Japan.

M. He was with the Department of Electrical and Communication Engineering, Tohoku University, Sendai 980-77, Japan. He is now with the Department of Electronic Engineering, Beijing Institute of Technology, Beijing 100081, China (e-mail: hemang@bit.edu.cn).

L. Wang, Q. Chen, Q. Yuan, and K. Sawaya are with the Department of Electrical and Communication Engineering, Tohoku University, Sendai 980-77, Japan (e-mail: chenq@ecei.tohoku.ac.jp).

Color versions of one or more of the figures in this paper are available online at http://ieeexplore.ieee.org.

Digital Object Identifier 10.1109/TMTT.2010.2063850

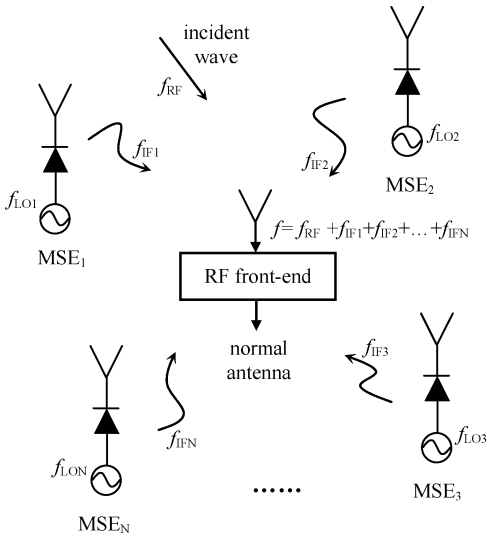

Fig. 1. Configuration of the MSAA loaded with diodes.

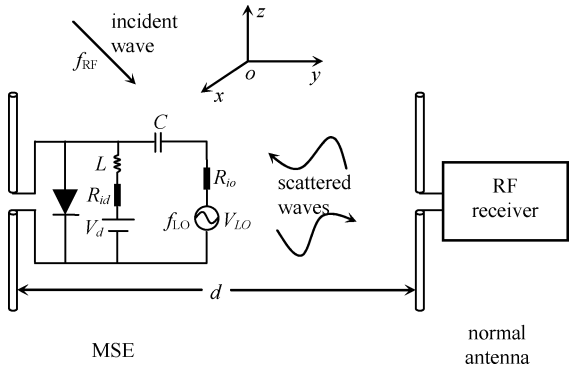

Fig. 2. Structure of a two-element MSAA loaded with a Schottky diode.

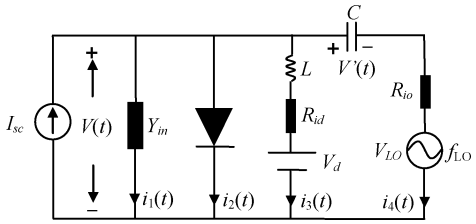

Fig. 3. Equivalent circuit of the MSE under incident electromagnetic (EM) wave.

is connected to the RF receiver. Thus, the received signals at the normal receiving antenna have an infinite number of frequencies $f_{\rm IF} = mf_{\rm RF} \pm nf_{{\rm LO}i}$ $(m, n = 0, 1, 2, \ldots,$ and $i = 1, 2, \ldots, N)$ since the local signal frequency for each MSE may be distinct. These received signals can be used for adaptive combination in the RF receiver by tuning the corresponding weight for each receiving signal.

In the MSAA, the normal receiving antenna and the MSEs can be of any type, their relative positions are arbitrary, and the nonlinear devices can also be selected with great freedom. In particular applications, all these parameters could be adjusted to optimize the performance of the MSAA. Therefore, the MSAA may be a very flexible and attractive candidate as the receiving antenna array in MIMO systems [4]. More important, only one branch of the RF receiver is needed in the MSAA. This feature makes the MSAA be very appealing when it is used for the mobile terminals in MIMO systems where compactness and energy saving are of primary concerns.

B. Analysis Method Based on Volterra Series and MoM

In [2]–[4], extensive experiments have been conducted to study the applicability of the MSAA for mobile handsets, where the second-order intermodulation scattering field was used as the modulated signal. It was found that the performance of the MSAA was slightly inferior to that of the normal receiving array antenna whose elements are all half-wavelength dipoles without any nonlinear device. The main reason is that the power level of the modulated scattering from MSEs with the frequency $f_{\rm IF}$ is much lower than that of the signal with the frequency $f_{\rm RF}$ appearing at the normal receiving antenna due to direct incidence. Such power level imbalance apparently degrades the performance of the MSAA [2].

In this section, for the first time, we will investigate the performance of a two-element MSAA from the theoretical point of view. Although the analysis procedure is demonstrated for the two-element array case for brevity, it can be easily extended to an MSAA of an arbitrary number of elements in a straightforward manner. The structure of a two-element MSAA loaded with Schottky diode is shown Fig. 2. V_d and $V_{\rm LO}$ are the dc bias and the local signal voltages, while R_{id} and R_{io} are the internal resistors of the corresponding signal generators, respectively. L and C are the RF choke inductance and dc block capacitance, respectively. The MSAA resides at the *yoz*-plane under the plane-wave incidence with frequency $f_{\rm RF}$, and the distance between two array elements is d.

The equivalent circuit for the MSE is shown in Fig. 3 by using the similar procedures in [5]–[7]. $I_{\rm sc}$ is the short-circuited current at the port of the MSE at $f_{\rm RF}$, and $Y_{\rm in}$ is the input admittance of the MSE without loading. Both $I_{\rm sc}$ and $Y_{\rm in}$ are calculated in the presence of the normal receiving antenna, therefore the effect of mutual coupling between the MSE and the normal antenna element is included. According to Kirchhoff's current law (KCL), following equations are established:

$$i_1(t) + i_2(t) + i_3(t) + i_4(t) = I_{\rm sc} \tag{1}$$

where

$$\begin{cases} i_1(t) = Y_{\rm in} V(t) \\ i_2(t) = f[V(t)] \\ V_d + i_3(t) R_{id} + L\dfrac{di_3(t)}{dt} = V(t) \\ V_{\rm LO} + i_4(t) R_{io} + V'(t) = V(t) \\ i_4(t) = C\dfrac{dV'(t)}{dt} \end{cases} \tag{2}$$

and $f[\cdot]$ is the i–v characteristics of the nonlinear device. For a typical Schottky diode [8],

$$i(t) = f[V(t)] = I_s\left(e^{\alpha V(t)} - 1\right) = I_s\left(e^{V(t)/V_t} - 1\right) \tag{3}$$

I_s is the reverse saturation current and $V_t = 1/\alpha$ and α depends on the structure of the diode. Replacing (2) into (1), we obtain

$$Y_{\text{in}}V(t) + f[V(t)] + \left[V(t) - V_d - L\frac{di_3(t)}{dt}\right] \Big/ R_{id} + [V(t) - V_{\text{LO}} - V'(t)]/R_{io} = I_{\text{sc}}. \quad (4)$$

Further, the time-domain voltage and current can be decomposed into the dc part V_0 and the dynamic part $v(t)$ due to the existence of dc block capacitance and RF choke inductance. These are expressed as

$$V(t) = V_0 + v(t) \quad (5)$$

where V_0 and $v(t)$ are dc and time-varying parts of $V(t)$, respectively. Thus, (3) becomes

$$\begin{aligned} i(t) &= f[V(t)] \\ &= f[V_0 + v(t)] \\ &= f[V_0] + \left.\frac{df}{dV}\right|_{V=V_0} v(t) + \frac{1}{2}\left.\frac{d^2f}{dV^2}\right|_{V=V_0} \\ &\quad \times v^2(t) + O(v^3(t)) \\ &= I_0 + \left.\frac{df}{dV}\right|_{V=V_0} v(t) + \frac{1}{2}\left.\frac{d^2f}{dV^2}\right|_{V=V_0} \\ &\quad \times v^2(t) + O(v^3(t)). \end{aligned} \quad (6)$$

Let

$$a_1 = \left.\frac{\partial f}{\partial V}\right|_{V=V_0} \qquad a_2 = \frac{1}{2}\left.\frac{\partial^2 f}{\partial V^2}\right|_{V=V_0} \quad (7)$$

and

$$i_2'(t) = a_1 v(t) + a_2 v^2(t). \quad (8)$$

Equation (6) then becomes

$$i(t) = I_0 + i_2'(t) = I_0 + a_1 v(t) + a_2 v^2(t). \quad (9)$$

Therefore, (4) can be rewritten as follows.
For the dc part,

$$I_0 + \frac{(V_0 - V_d)}{R_{id}} = 0 \quad (10)$$

and for the dynamic part,

$$Y_{\text{in}}v(t) + i_2'(t) + G_{io}v(t) = I_{\text{sc}} + G_{io}V_{\text{LO}} \quad (11)$$

where $G_{io} = 1/R_{io}$. In (10) and (11), the current and voltage involving L and C are neglected since their contributions are much smaller compared to other terms. Therefore, the equivalent circuit of the MSE can also be decoupled into two sub-circuits: one is the dc-bias circuit and the other one is the time-varying circuit, as shown in Fig. 4. It is noted that we have used the first three terms in the Taylor-series expansion of $f[\cdot]$ in (6).

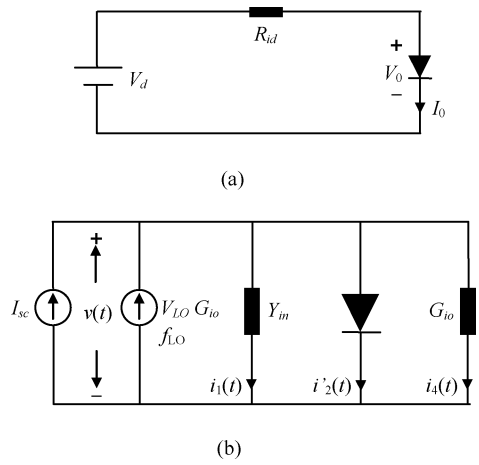

Fig. 4. DC bias and dynamic sub-circuits of the MSE under the incident EM wave. (a) DC-bias sub-circuit. (b) Dynamic sub-circuit.

Hence, our analysis is based on the small-signal approximation, but it is accurate enough for modeling MSAA application in the wireless communication system.

For the analysis of the nonlinear circuit in Fig. 4, there exists a variety of approaches [5]–[7], [9]. The Volterra-series method is employed in this paper due to its closed-form formulation for the final output that could provide clear physical insights of the performance of MSAA, although other purely numerical approaches could produce more accurate results if strong nonlinearities are considered [6], [7]. Another advantage of this choice is that Volterra analysis can be implemented entirely in the frequency domain without the use of the fast Fourier transform (FFT) [5], [9].

Fig. 4(b) is a two-tone excited nonlinear circuit. The short-circuited current I_{sc} and the voltage V_{LO} of the local signal are written in the frequency domain as follows:

$$\begin{aligned} I_{\text{sc}} &= \text{Re}\left(|\vec{I}|e^{j(\omega_1 t + \varphi)}\right) \\ &= |\vec{I}|\cos(\omega_1 t + \varphi) \\ &= \frac{1}{2}[\vec{I}e^{j\omega_1 t} + \vec{I}^* e^{-j\omega_1 t}] \end{aligned} \quad (12)$$

and

$$V_{\text{LO}} = \vec{V}_L \cos(\omega_2 t) = \frac{1}{2}[\vec{V}_L e^{j\omega_2 t} + \vec{V}_L e^{-j\omega_2 t}] \quad (13)$$

where $\omega_1 = 2\pi f_{\text{RF}}, \omega_2 = 2\pi f_{\text{LO}}$, and $\vec{I}$ and $\vec{V}_L$ are the phasor representations of I_{sc} and V_{LO}, respectively. In (13), the initial phase of $\vec{V}_L$ is assumed to be zero.

Substituting (12) and (13) in (11), we obtain

$$Y_{\text{in}}v(t) + i_2'(t) + G_{io}v(t) = \frac{1}{2}[\vec{I}e^{j\omega_1 t} + \vec{I}^* e^{-j\omega_1 t}] + \frac{1}{2}[G_{io}\vec{V}_L e^{j\omega_2 t} + G_{io}\vec{V}_L e^{-j\omega_2 t}]. \quad (14)$$

Let

$$\vec{E}_{-1} = \vec{I}^*, \vec{E}_1 = \vec{I}, \vec{E}_{-2} = \vec{E}_2 = G_{io}\vec{V}_L \tag{15}$$

where the superscript "*" denotes the complex conjugate. The excitation signal on the right-hand side of (14) becomes

$$\begin{aligned} x(t) &= \frac{1}{2}\vec{E}_{-1}e^{-j\omega_1 t} + \frac{1}{2}\vec{E}_1 e^{j\omega_1 t} + \frac{1}{2}\vec{E}_{-2}e^{-j\omega_2 t} + \frac{1}{2}\vec{E}_2 e^{j\omega_2 t} \\ &= \frac{1}{2}\sum_{\substack{l=-2 \\ l\neq 0}}^{2} \vec{E}_l e^{-j\omega_l t}. \end{aligned} \tag{16}$$

According to Volterra analysis [9], [5], the output voltage $v(t)$ in Fig. 4(b) can be expressed by a series whose term is the product of the frequency-domain excitation signals and the transfer functions for the nonlinear circuit

$$\begin{aligned} v(t) = &\frac{1}{2}\sum_{\substack{l=-2 \\ l\neq 0}}^{2} \vec{E}_l H_1(\omega_l) e^{j\omega_l t} \\ &+ \frac{1}{4}\sum_{l_1=-2}^{2}\sum_{\substack{l_2=-2 \\ l_p\neq 0}}^{2} \vec{E}_{l_1}\vec{E}_{l_2} H_2(\omega_{l_1}, \omega_{l_2}) e^{j(\omega_{l_1}+\omega_{l_2})t} \end{aligned} \tag{17}$$

where $p = 1, 2$, and $H_1(\omega_l)$ and $H_2(\omega_{l_1}, \omega_{l_2})$ are the first- and second-order transfer functions, respectively. In (17), the negative frequencies are defined as

$$\omega_{-l} = -\omega_l. \tag{18}$$

It is noted that only up to second-order responses have been considered in (17) because the modulated scattering signal used in the MSAA is the second-order mixing product with the frequency $f_{\rm IF} = f_{\rm RF} - f_{\rm LO}$ caused by the nonlinear diode [2]–[4]. This means that MSAA only utilizes the weak nonlinearities of the nonlinear device. The contributions from the higher order nonlinearities to the output at the frequency $f_{\rm IF}$ can also be included in the analysis, at the expense of computation complexity, but their effects are much smaller compared to the second-order intermodulation. Therefore, (17) could depict the second-order modulated signal without appreciable accuracy limitation in the small-signal wireless communication scenario.

The transfer functions are found by exciting the circuit in Fig. 4(b) at two frequencies, ω_1 and ω_2, and calculating the output voltages at the frequencies ω_1 and $\omega_1 - \omega_2$. The final results of the first- and second-order transfer functions are

$$H_1(\omega) = \frac{1}{A(\omega)} \tag{19a}$$

and

$$\begin{aligned} H_2(\omega_1, -\omega_2) &= -a_2 H_1(\omega_1) H_1^*(\omega_2) H_1(\omega_1 - \omega_2) \\ &= \frac{-a_2}{A(\omega_1)A^*(\omega_2)A(\omega_1 - \omega_2)} \end{aligned} \tag{19b}$$

where $A(\omega)$ is the linear admittance of the shunt circuit shown in Fig. 4(b)

$$A(\omega) = Y_{\rm in}(\omega) + G_{io} + a_1. \tag{20}$$

In the derivation of (19a) and (19b), following relations of the transfer functions have been used:

$$\begin{cases} H_1(-\omega) = H_1^*(\omega) \\ H_2(-\omega_1, \omega_2) = H_2^*(\omega_1, -\omega_2) \\ H_2(\omega_1, \omega_2) = H_2(\omega_2, \omega_1). \end{cases} \tag{21}$$

Finally, the frequency-domain output voltages of the circuit Fig. 4(b) at ω_1 and $\omega_1 - \omega_2$ are

$$v(\omega_1) = \vec{E}_1 H_1(\omega_1) \tag{22}$$

and

$$v(\omega_1 - \omega_2) = \vec{E}_1\vec{E}_{-2} H_2(\omega_1, -\omega_2). \tag{23}$$

In summary, the analysis procedures of the Schottky diode loaded two-element MSAA are organized as follows.

Step 1) Solve the nonlinear equation (10) to obtain the dc-bias voltage V_0 at the terminal of diode.

Step 2) According to (3) and (7), obtain the coefficients a_1 and a_2.

Step 3) At the frequency ω_1, calculate the input admittance $Y_{\rm in}(\omega_1)$ of the MSE in the presence of the normal receiving antenna using the MoM [10], and then compute the shunt admittance $A(\omega_1)$ of the circuit Fig. 4(b) using (20).

Step 4) Compute $A(\omega_2)$ at ω_2 using the method similar to that in Step 3).

Step 5) Compute $A(\omega_1 - \omega_2)$ at $\omega_1 - \omega_2$ by using the same method as in Step 3).

Step 6) Calculate the short-circuited current $\vec{I}$ of the MSE without loading at ω_1 in the presence of the normal receiving antenna by using the MoM. Then obtain the excitation phasors $\vec{E}_l (l = -2, -1, 1, 2)$ according to (15).

Step 7) Calculate the output voltages $v(\omega_1)$ and $v(\omega_1 - \omega_2)$ at the terminal of the MSE by using (22) and (23).

Step 8) Finally, calculate the received power $P_{\rm RF}$ by the normal receiving antenna as the summation of the direct incidence and the scattering from the MSE caused by $v(\omega_1)$ at the frequency ω_1, and the received power $P_{\rm IF}$ at $\omega_1 - \omega_2$ from MSE due to the reradiation of $v(\omega_1 - \omega_2)$.

In fact, the radiation produced by $v(\omega_1)$ and $v(\omega_1 - \omega_2)$ from the MSE will be reflected by the normal receiving antenna again, and these reflected waves will excite new mixing products with infinite frequencies including ω_1 and $\omega_1 - \omega_2$. The multiple reflections between the elements in the MSAA will proceed until the ultimate equilibrium is reached. However, the contributions from these multireflection effects to the final received power levels at ω_1 and $\omega_1 - \omega_2$ are higher order quantities compared to the first-order reradiation of $v(\omega_1)$ and $v(\omega_1 - \omega_2)$ from the MSE as calculated in the above procedures. Therefore, they are neglected in Step 8) for efficient and fast computation without much loss of accuracy.

C. Discussion

As been pointed out before, the performance of the MSAA can be improved by enhancing the received power $P_{\rm IF}$ of the

modulated scattering signal. Thus, it is important and interesting to exploit the approaches to increase $P_{\rm IF}$. According to the analysis presented in Section II-B, this power level is determined by $v(\omega_1-\omega_2)$. Replace (19b) and (20) into (23), $v(\omega_1-\omega_2)$ can be rewritten as

$$v(\omega_1-\omega_2)=-\vec{I}\cdot\vec{V}_L\cdot G_{io}a_2 \cdot\frac{1}{[Y_{\rm in}(\omega_1)+G_{io}+a_1][Y_{\rm in}^*(\omega_2)+G_{io}+a_1]} \cdot\frac{1}{[Y_{\rm in}(\omega_1-\omega_2)+G_{io}+a_1]}. \quad (24)$$

From (24), the following means could be adopted in order to increase the level of $P_{\rm IF}$ for the fixed internal admittance G_{io} of the local signal generator.

- Optimize the coefficients a_1 and a_2 by tuning the dc-bias voltage V_d to increase $P_{\rm IF}$ level, which means that the circuit should work at an appropriate driving point of the diode.
- Adjust the short-circuited current $\vec{I}$ of the MSE at ω_1 and the input admittance $Y_{\rm in}$ of the MSE without loading at ω_1, ω_2, and $\omega_1-\omega_2$ in the presence of the normal antenna, which can be realized through the following.
  - Modifying the shape of the MSE for given types of the MSE and the normal receiving antenna (e.g., we can change the length of MSE if it is a metallic thin-wire scatterer).
  - Loading the diode at different positions in the MSE.
  - Choosing a suitable frequency ω_2 of the local signal that can reradiate the second-order modulated signal at $\omega_1-\omega_2$ more effectively.
- Increasing the magnitude of the local signal since $v(\omega_1-\omega_2)$ is linearly proportional to $\vec{V}_L$. However, the effect will be limited to the small-signal regime because the saturation will occur if it is too large.

By virtue of the simple expression of (24) resulting from Volterra analysis, the above guidelines give us some useful physical insights to optimize the behavior of the MSAA. However, any parameter in (24) is not independent of others. Therefore, we will investigate the feasibility of the proposed theoretical analysis in Section III through numerical simulations and experimental validations.

III. Parametrical Studies

In this section, we will carry out the numerical parametrical study to maximize the receiving power $P_{\rm IF}$ in the MSAA by using an in-house MoM code [11] combined with Volterra analysis, as presented in Section II firstly, and then experiments are conducted to validate the numerical simulations. The geometry of the two-element MSAA is shown in Fig. 5, where the normal receiving antenna is a half-wavelength dipole at frequency $f_{\rm RF}$, while the MSE is chosen as a thin-wire scatterer loaded with a Schottky diode and relevant circuits. The length of the MSE is l and the loading position measured from the center of the thin wire is s. The entire structure is within the *yoz*-plane, and the distance between two elements is d with the coordinate origin being the midpoint. A vertically polarized plane wave

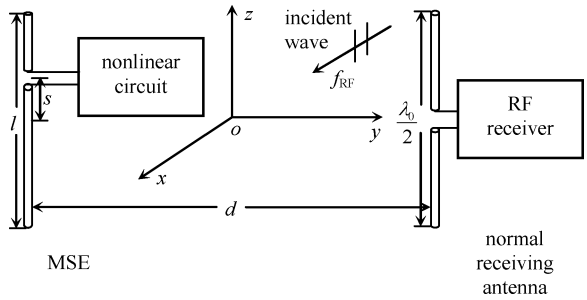

Fig. 5. Geometry of the two-element MSAA with a half-wavelength dipole receiving antenna and a thin-wire-like MSE loaded with a Schottky diode.

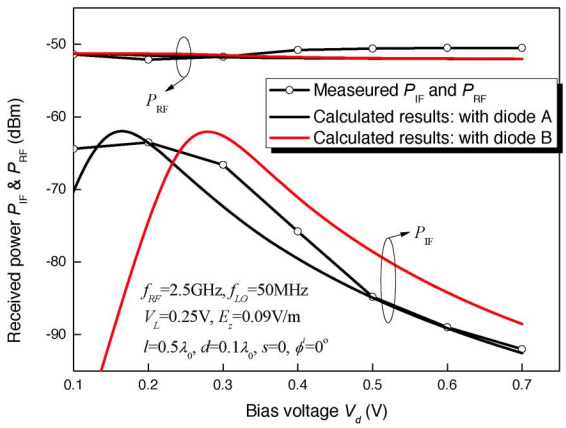

Fig. 6. Measured and calculated received power $P_{\rm IF}$ and $P_{\rm RF}$ with various diode parameters under different dc-bias voltages.

TABLE I
Parameters of Diode A and B

	Diode A	Diode B
V_t	25.0 mV	25.0 mV
I_s	1.0 μA	10.0 nA

$\vec{E}^i=\hat{z}E_z e^{-j(kx\cos\varphi^i+ky\sin\varphi^i)}$ with the frequency $f_{\rm RF}$ is assumed as the excitation signal of the MSAA, where φ^i is the angle of the propagation vector with respect to the $+x$-direction. The configuration of nonlinear circuit connected to the MSE is shown in Fig. 2. In the simulations, we set the internal resistors R_{id} and R_{io} of the signal generators and the input impedance of the RF receiver to be 50 Ω, and both the dipole antenna and MSE having the length-diameter ratio of 74.2.

A. Effect of the Driving Point of the DC-Bias Circuit

First, we investigate the effect of the different driving point of the dc-bias circuit on the received power level at ω_1 and $\omega_1-\omega_2$. Fig. 6 shows the calculated $P_{\rm IF}$ and $P_{\rm RF}$ with two different typical diodes versus various bias voltages under the front incident ($\varphi^i=0°$) plane wave. The parameters of diode A and B are listed in Table I and other parameters used in the simulation are shown in Fig. 6, where V_L is the magnitude of local signal voltage and λ_0 is the wavelength in free space at $f_{\rm RF}$.

It is found that the scattered signal levels rise rapidly with the increasing V_d, and then fall at a slower speed after reaching its maximum. $P_{\rm RF}$ remains almost constant with different diode

TABLE II
MAXIMUM $P_{\rm IF}$ AND THE CORRESPONDING BIAS VOLTAGE AND CONSUMED POWER OF DC CIRCUIT FOR VARIOUS DIODE TYPES AND ELEMENT DISTANCE POWER UNIT: DBM, VOLTAGE UNIT: V, DISTANCE UNIT: λ_0

	Diode Type A				Diode Type B			
d	$P_{\rm IF}$	$P_{\rm RF}$	V_d	$P_{\rm DC}$	$P_{\rm IF}$	$P_{\rm RF}$	V_d	$P_{\rm DC}$
0.1	-62.4	-51.3	0.15	-14.3	-62.6	-51.5	0.3	-7.9
0.5	-67.2	-44.6	0.15	-14.3	-67.8	-44.7	0.3	-7.9
1.0	-74.3	-49.7	0.15	-14.3	-74.9	-49.5	0.3	-7.9

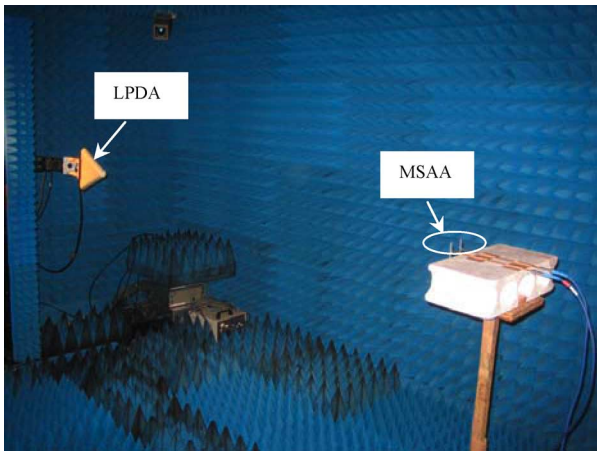

Fig. 7. Experiment setup in the anechoic chamber.

parameters and bias voltages, which means that $P_{\rm RF}$ is dominated by direct incidence and the contribution of the reradiation from the MSE is small. Moreover, maximum $P_{\rm IF}$ occurs at a lower bias voltage (about 0.15 V) when the diode is of type A, which has steeper i–v characteristics (larger I_s) compared to diode B. For other incidence direction φ^i and element distance d, a similar phenomenon is also observed. Therefore, a Schottky diode with a larger saturation current is preferred in the MSAA for the purpose of power saving if other parameters of the diode remain fixed. Table II shows the consumed power of the dc-bias circuit at the point where the maximum $P_{\rm IF}$ occurs by using two different types of the diodes and various element distances. It is clear that the consumed power $P_{\rm DC}$ of the dc-bias circuit with diode A is much less than that with diode B and the maximum received $P_{\rm IF}$ are almost same in both cases.

To validate the numerical results, an experiment is carried out in the anechoic chamber. In the experimental setup, as shown in Fig. 7, a log-periodic dipole array (LPDA) (electro-Metrics EM6952) is used as the transmitting antenna and is 3.0 m away from the MSAA. At the transmitting frequency 2.5 GHz, this distance is large enough to guarantee that the MSAA is in the far field of the LPDA and that the radiating wave is nearly a local vertically polarized plane wave when it impinges the MSAA. The LPDA is fed by an Agilent E4438C ESG vector signal generator and the input power is set to be -5 dBm. At the receiving end, the MSE is a half-wavelength (at 2.5 GHz) thin-wire conductor loaded with a Schottky diode HSC276 from Renesas Ltd., and a two-channel multifunction synthesizer (NF WF 1966) is connected to the MSE as the local signal generator with the frequency of 50 MHz. While the normal receiving antenna is a half-wavelength dipole, followed by a real-time spectrum analyzer (Tektronix RSA3308A) that is used to measure

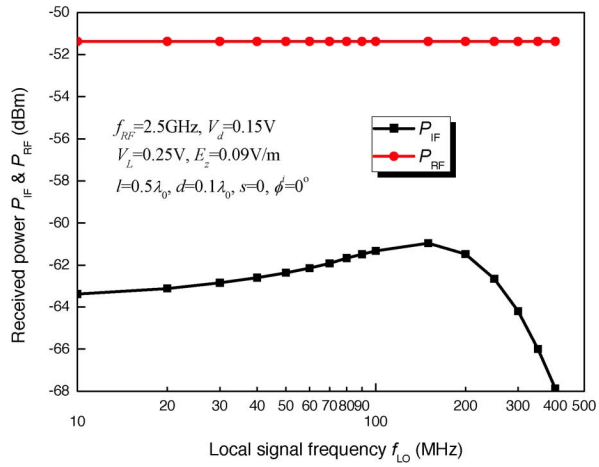

Fig. 8. Simulated received power $P_{\rm IF}$ and $P_{\rm RF}$ by using various local signal frequencies.

the received power levels $P_{\rm IF}$ at $\omega_1 - \omega_2$ (2.45 GHz) and $P_{\rm RF}$ at ω_1 (2.5 GHz).

It is worth mentioning that, in the numerical simulations, the calculated received power $P_{\rm RF}$ at ω_1 are firstly adjusted to match the first measured power level from the spectrum analyzer (when the bias voltage V_d is 0.1 V in Fig. 6) by simply tuning the magnitude of the incident plane wave E_z to 0.09 V/m in the code since we do not know the exact power density of the incident wave at the MSAA. This value of E_z is then used throughout the following numerical simulations. The above tuning process of E_z can be considered as a numerical calibration. The parameters a_1 and a_2, which characterize the Schottky diode, are not measured in the experiment and two typical values α [8] for the Schottky diode type A and B (see Table I) are used in all numerical simulations. It is found that the measured result presented in Fig. 6 shows reasonable agreement with the calculated one for the MSAA loaded with diode A, the relative error of the maximum $P_{\rm IF}$ is less than 3%, which means the characteristics of the diode HSC276 is close to the typical Schottky diode with the parameters $I_s = 1.0$ μA and $V_t = 25$ mV. The measured bias voltage for maximum $P_{\rm IF}$ is around 0.15 V, which matches well to the numerical prediction (for diode A).

B. *Effect of Local Signal Frequency*

Fig. 8 shows the numerical results of the received power level at ω_1 and $\omega_1 - \omega_2$ by tuning the local signal frequency $f_{\rm LO}$ for the MSE from 10 to 400 MHz under the front incident plane wave with vertical polarization. It is seen that the local signal frequency has a minor effect on $P_{\rm RF}$ and $P_{\rm RF}$ remains almost constant. However, the received power $P_{\rm IF}$ increases slowly when $f_{\rm LO}$ is changed from 10 to 150 MHz, and decreases rapidly when $f_{\rm LO}$ is beyond 150 MHz. The maximum $P_{\rm IF}$ occurs when $f_{\rm LO}$ is 150 MHz. At this frequency, the length of the thin-wire MSE is about 0.47 wavelengths at $\omega_1 - \omega_2$, which exhibits the strongest reradiation ability of the second-order mixing signal from the diode. A similar phenomenon is also observed when the distance d and incident angle φ^i are changed to other values.

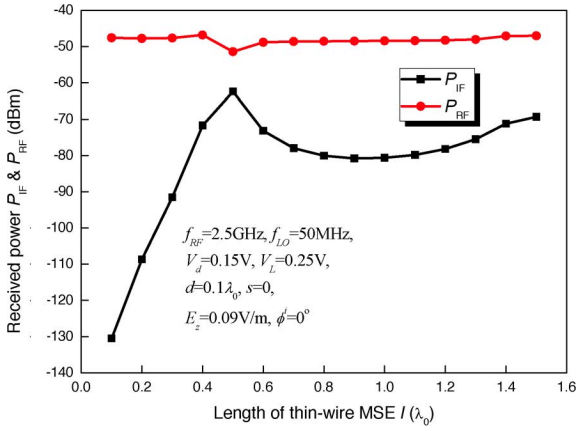

Fig. 9. Simulated received power P_{IF} and P_{RF} with different thin-wire MSE lengths.

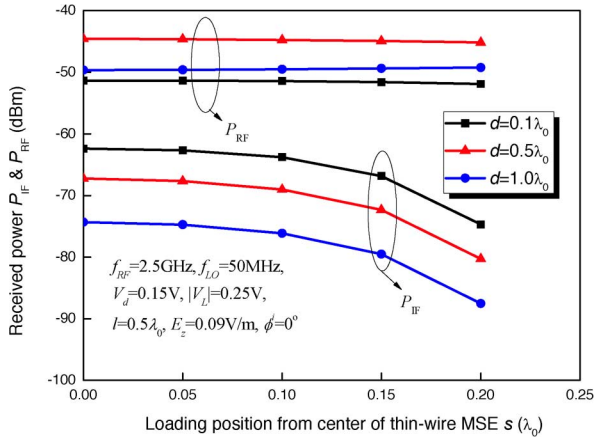

Fig. 10. Simulated received power P_{IF} and P_{RF} when the diode is loaded at different positions along the thin-wire MSE.

C. Effect of the Length of Thin-Wire MSE

The effects of the thin-wire MSE length on the received power level are investigated by numerical simulations. An apparent resonance is found in Fig. 9 when the length of the MSE is about 0.5 wavelengths at ω_1, which means strong mutual coupling occurs between the elements of MSAA at this length. It is also noticed that the level of P_{IF} is very low if the length of the MSE is much shorter than a half-wavelength. A second resonance will also happen if we increase l to about 1.5 λ_0, but the MSE of such a length is of little useful applications in the mobile terminals when compactness is considered in the communication system design.

D. Effect of Loading Position in the MSE

It is well known that the loading position of the linear or nonlinear device on antenna plays an important role in determining the radiation and scattering properties of the loaded antenna structure. The effect of the loading position of the Schottky diode along the MSE on the received power levels in MSAA system is demonstrated in Fig. 10. For three different element distances, the received power P_{IF} at $\omega_1 - \omega_2$ is reduced monotonically when the loading point approaches to the end of the thin-wire MSE, while P_{RF} is only changed slightly. Clearly, the center-loaded MSE should be chosen in the MSAA in order to produce maximum P_{IF}.

E. Effect of the Magnitude of the Local Signal in MSE

As been pointed out in Section II, $v(\omega_1 - \omega_2)$ is linearly proportional to the local signal voltage V_L in the small-signal scenario. Fig. 11 shows the relation between the received power level and the magnitude of the local signal voltage through both experiments and numerical simulations. It can be seen from Fig. 11 that the numerical results agree well with the measured ones and the maximum error is less than 1.5 dB (the relative error is less than 2.5%) in the small-signal regime ($0 < V_L < 0.25$ V). Within this voltage range, P_{IF} is increased by about 6 dB when V_L is doubled, and P_{RF} remains almost unchanged since it is dominated by direct incidence. When V_L exceeds 0.25 V, the measured P_{IF} remains almost constant due to the saturation of the diode. However, the simulated P_{IF} based on the present theoretical analysis will increase continuously because of the limitation of Volterra analysis for strong nonlinearities prediction [9].

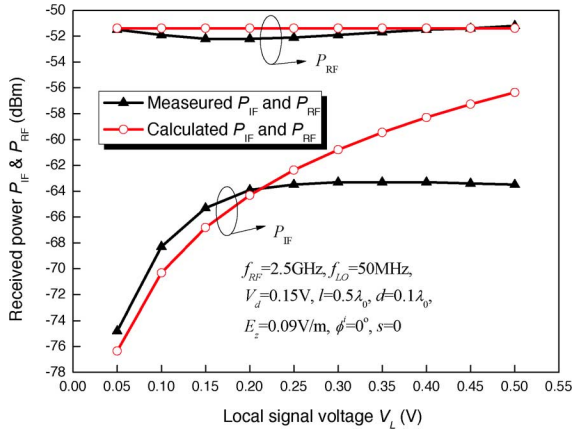

Fig. 11. Measured and simulated received power P_{IF} and P_{RF} versus various local signal voltage of the MSE.

F. Effect of the Distance Between the MSAA Elements

The measured and simulated received power levels of the MSAA at $\omega_1 - \omega_2$ versus various distances between the elements, under the vertically polarized incident plane wave from front direction, are shown in Fig. 12. Reasonable agreement of two types of results is observed, and the largest error is less than 2 dB (the relative error is less than 3.4%). P_{IF} decreases rapidly and then changes only slightly when d is of intermediate value ($0.3\ \lambda_0 < d < 0.7\ \lambda_0$), indicating complicated interaction between two elements of the MSAA in this distance range, and decreases monotonically again with a large element distance where the mutual coupling becomes weak. Furthermore, Fig. 13 shows the relation of the received power level and the element distance when the plane wave impinges the MSAA from different directions. It is noticed that P_{IF} and P_{RF} curves have quite different shapes when φ^i changes, which means the performance of the MSAA is a strong function of the incident angle. More interestingly, P_{IF} exceeds P_{RF} if d is small and the plane wave illuminates the MSAA from the MSE side ($\varphi^i = 90°$).

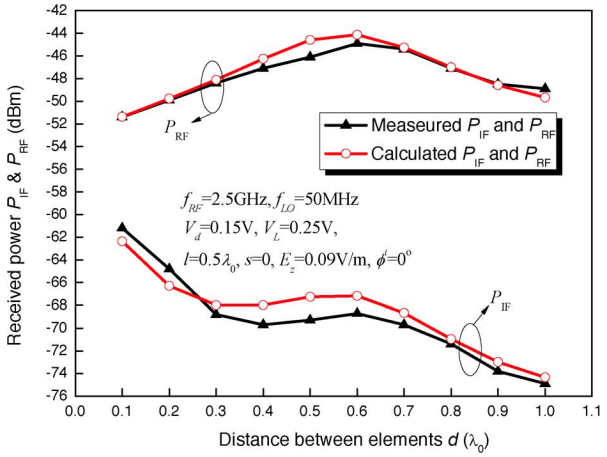

Fig. 12. Measured and calculated received power P_{IF} and P_{RF} versus various distances between MSAA elements.

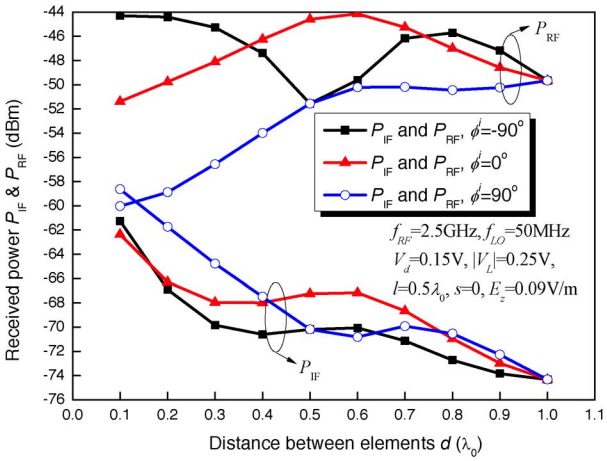

Fig. 13. Simulated received power P_{IF} and P_{RF} versus distances between MSAA elements under various incident angles.

In such a case, the MSE blocks the incident wave and subsequently reduces the power received by the normal receiving antenna due to direct incidence. Therefore, the distance between the MSE and the normal receiving antenna can be adjusted according to the relative power requirement of two signals in the MSAA system.

G. Discussion of Uncertainties

As seen from the above theoretical and experimental results, there are small discrepancies between the measured controls and simulated results. We consider that these uncertainties are mainly due to the following factors.

1) Since we cannot find a way to obtain the exact reverse saturation current I_s, the exact value of V_t, and the true i–v relation of the diode used in the experiment, the parameters a_1 and a_2 used in numerical simulations are derived using typical values of I_s and V_t and ideal i–v characteristics of Schottky diodes. The inaccuracy between the estimated and exact diode parameters is one of the main reasons for the discrepancy between the calculated results and measured ones.
2) The incident wave to the MSAA is not a perfect plane wave in the experiment, while in numerical simulations, the incident wave is an ideal plane wave. This inconsistence will also cause some errors between two kinds of results.
3) In the experiment, the nonideal free-space environments (cables, supporting foam for the MSAA, etc.) may affect the measured results to some extent.

IV. Conclusion

In this paper, an accurate and efficient theoretical scheme based on the Volterra analysis and the MoM has been proposed to investigate the performance of the MSAA with potential application to communication terminals in the MIMO systems. Experiments are conducted to validate the proposed theory, and the relative errors between the numerical results are within 5% for most results. The theoretical analysis gives clear relations of the nonlinear component parameters with the received power levels at two distinct frequencies, which may provide very useful guidelines to improve the performance of the MSAA system. More specifically, in order to increase the receiving power level of the second-order mixing product signal caused by the nonlinear diode, we can choose an optimal dc bias voltage to excite the MSE, appropriate local signal frequency and voltage magnitude, suitable length of the MSE, correct loading position to maximize the reradiation of the modulated signal, etc. Although the numerical and experimental results are illustrated only for the plane-wave incidence with fixed incident angles, the performance of the MSAA in realistic MIMO communication channels can also be predicted by using the proposed method in addition to the use of statistical approaches, which will be the focus of the authors' future work.

References

[1] J. H. Richmond, "A modulated scattering technique for measurement of field distribution," *IRE Trans. Microw. Theory Tech.*, vol. MTT-3, no. 4, pp. 13–15, Jul. 1955.
[2] Q. W. Yuan, M. Ishizu, Q. Chen, and K. Sawaya, "Modulated scattering array antennas for mobile handsets," *IEICE Electron. Exp.*, vol. 2, no. 20, pp. 519–522, Oct. 2005.
[3] Q. Chen, Y. Takeda, Q. W. Yuan, and K. Sawaya, "Diversity performance of modulated scattering array antenna," *IEICE Electron. Exp.*, vol. 4, no. 7, pp. 216–220, Apr. 2007.
[4] Q. Chen, L. Wang, T. Iwaki, Y. Kakinuma, Q. W. Yuan, and K. Sawaya, "Modulated scattering array antenna for MIMO applications," *IEICE Electron. Exp.*, vol. 4, no. 23, pp. 745–749, Dec. 2007.
[5] T. K. Sarkar and D. D. Weiner, "Scattering analysis of nonlinearly loaded antennas," *IEEE Trans. Antennas Propag.*, vol. AP-24, no. 3, pp. 125–131, Mar. 1976.
[6] C. C. Huang and T. H. Chu, "Analysis of wire scatterers with nonlinear or time-harmonic loads in the frequency domain," *IEEE Trans. Antennas Propag.*, vol. 41, no. 1, pp. 25–30, Jan. 1993.
[7] K. Sheshyekani, S. H. H. Sadeghi, and R. Moini, "A combined MoM–AOM approach of nonlinearly loaded antennas in the presence of a lossy ground," *IEEE Trans. Antennas Propag.*, vol. 56, no. 6, pp. 1717–1724, Jun. 2008.
[8] D. M. Pozar, *Microwave Engineering*, 3rd ed. New York: Wiley, 2005.
[9] S. A. Mass, *Nonlinear Microwave and RF Circuits*, 2nd ed. Boston, MA: Artech House, 2003.
[10] R. F. Harrington, *Field Computation by Moment Methods*. New York: Wiley, 1993.
[11] M. He, "On the characteristics of radome enclosed archimedean spiral antennas," *IEEE Trans. Antennas Propag.*, vol. 56, no. 7, pp. 1867–1874, Jul. 2008.

Mang He (M'09) received the B.S. and Ph.D. degrees in electrical engineering from the Beijing Institute of Technology, Beijing, China, in 1998 and 2003, respectively.

From September 1998 to July 2003, he was a Graduate Research Associate with the Antenna and Propagation Laboratory, Beijing Institute of Technology. Since 2006, he has been an Associate Professor with the Beijing Institute of Technology. From September 2003 to September 2004, he was a Research Associate with the Department of Electronic Engineering, City University of Hong Kong. From May 2008 to March 2009, he was with the Department of Electrical and Communication Engineering, Tohoku University, Sendai, Japan, as a Postdoctoral Research Fellow. His research interests include computational electromagnetics, conformal microstrip antennas, and electromagnetic theory.

Lin Wang received the B.E. degree from the Shenyang Institute of Chemical Technology, Shenyang, China, in 2006, the M.E. degree from the Tohoku University, Sendai, Japan, in 2009, and is currently working toward the Ph.D. degree in electrical and communication engineering at Tohoku University.

His research interests include diversity, MIMO wireless communications, and antenna measurement.

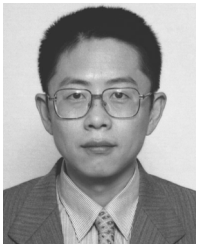

Qiang Chen (M'97) received the B.E. degree from Xidian University, Xi'an, China, in 1986, and the M.E. and D.E. degrees from Tohoku University, Sendai, Japan, in 1991 and 1994, respectively.

He is currently an Associate Professor with the Department of Electrical Communications, Tohoku University. He has been an Associate Editor of the *IEICE Transactions on Communications* since 2007. His primary research interests include computational electromagnetics, array antennas, and antenna measurement.

Dr. Chen is a member of the IEEE and Institute of Electronics, Information and Communication Engineers (IEICE), Japan. He was the secretary and treasurer of the IEEE Antennas and Propagation Society (IEEE AP-S) Japan Chapter in 1998, the secretary of the Technical Committee on Electromagnetic Compatibility, IEICE from 2004 to 2006, the secretary of the Technical Committee on Antennas and Propagation, IEICE from 2008 to 2010. He was the recipient of the 1993 Young Scientists Award and the 2009 Best Paper Award and 2009 Zen-ichi Kiyasu Award of the IEICE.

Qiaowei Yuan received the B.E., M.E., and Ph.D. degrees from Xidian University, Xi'an, China, in 1986, 1989 and 1997, respectively.

From 1990 to 1991, she was a Special Research Student with Tohoku University, Sendai, Japan. From 1992 to 1995, she was with Sendai Research and Development Laboratories, Matsushita Communication Company, Ltd., where she was engaged in research and design of the compact antennas for second-generation mobile phones. From 1997 to 2002, she was a researcher with the Sendai Research and Development Center, Oi Electric Company Ltd., where she was engaged in the research and design of small antennas for pager communication and the parabolic antenna for 26.5-GHz fixed wireless access (FWA) communication. From 2002 to 2007, she was a Researcher with the Intelligent Cosmos Research Institute, Sendai, Japan, where she was involved in the research and development of adaptive array antennas and RF circuits for mobile communications. From 2007 to 2008, she was an Associate Professor with the Tokyo University of Agriculture and Technology. She is currently an Associate Professor with the Sendai National College of Technology.

Dr. Yuan was the recipient of the 2009 Best Paper Award and 2009 Zen-ichi Kiyasu Award of the Institute of Electronics, Information and Communication Engineers (IEICE), Japan.

Kunio Sawaya (SM'02) received the B.E., M.E., and Ph.D. degrees from Tohoku University, Sendai, Japan, in 1971, 1973 and 1976, respectively.

He is currently a Professor with the Department of Electrical and Communication Engineerin, Tohoku University. His areas of interests are antennas in plasma, antennas for mobile communications, theory of scattering and diffraction, antennas for plasma heating, and array antennas.

Dr. Sawaya is a Fellow of the Institute of Electronics, Information and Communication Engineers (IEICE), Japan. He is a member of the Institute of Image Information and Television Engineers of Japan. From 2001 to 2003, he was the chairperson of the Technical Group of Antennas and Propagation, IEICE. He was the chairperson of the Organizing and Steering Committees of the 2004 International Symposium on Antennas and Propagation (ISAP'04) and the president of the Communications Society of IEICE from 2009 to 2010. He was the recipient of the 1981 Young Scientists Award, the 1988 Paper Award, the 2006 Communications Society Excellent Paper Award, and the 2009 Zen-ichi Kiyasu Award of the IEICE.